Mechanically interlocked stretchable nanofibers for multifunctional wearable triboelectric nanogenerator

Li, Yi; Xiong, Jiaqing; Lv, Jian; Chen, Jian; Gao, Dace; Zhang, Xiaoxing; Lee, Pooi See

2020

Li, Y., Xiong, J., Lv, J., Chen, J., Gao, D., Zhang, X., & Lee, P. S. (2020). Mechanically interlocked stretchable nanofibers for multifunctional wearable triboelectric nanogenerator. Nano Energy, 78, 105358. doi:10.1016/j.nanoen.2020.105358

https://hdl.handle.net/10356/143797

https://doi.org/10.1016/j.nanoen.2020.105358

Mechanically interlocked stretchable nanofibers for multifunctional wearable triboelectric nanogenerator

Yi Li [1, 2, #], Jiaqing Xiong [1, #], Jian Lv [1], Jian Chen [1], Dace Gao [1], Xiaoxing Zhang [2, 3 *] and Pooi See Lee [1, *]

[1] School of Materials Science and Engineering, Nanyang Technological University, 50 Nanyang Avenue, 639798, Singapore

[2] School of Electrical Engineering and Automation, Wuhan University, Wuhan, Hubei 430072, China

[3] Key Laboratory for High-Efficiency Utilization of Solar Energy and Operation Control of Energy Storage System, School of Electrical and Electronic Engineering, Hubei University of Technology, Wuhan 430068, China

[#] The authors contributed equally to this work.

[*] Corresponding author: pslee@ntu.edu.sg, xiaoxing.zhang@outlook.com

Abstract

Nanofibers with good softness and high surface specific area are excellent choices for wearable triboelectric nanogenerator (TENG), despite that the deformability and durability remain challenging in seamless integration with daily textiles/clothes. Herein, we propose a physical interlocking strategy to realize a self-interlocked stretchable, breathable and waterproof nanofibers-membrane by simultaneous electrospinning of poly (vinylidene fluoride-co-hexafluoropropylene) (PVDF-HFP) and electrospraying of styrene-ethylene-butylene-styrene (SEBS). The electrosprayed SEBS microspheres serve as the elastic binders and hydrophobic modifiers for enhancing stretchability and waterproofness of the electrospun PVDF-HFP fibers network. By means of a printable electrode consisted of liquid metal (gallium indium tin particles) and silver flakes, a stretchable nanofibers-based TENG (SNF-TENG) with high triboelectric output (85 V, 219.66 mW m^{-2}) and electrical durability was demonstrated, capable of harvesting energy from human motions and flowing water, powering 200 commercial LEDs and an electronic watch. The stretchable nanofibers membrane shows favorable mechanical compliance, which can be facilely integrated onto a stretchable textile to fabricate textile-TENG, promising for comfortable wearable applications for

power sources, smart raincoat, self-powered e-skin and tactile interactive interfaces.

Key Words: mechanically interlocked, stretchable nanofiber, breathable, waterproof, triboelectric nanogenerator, electronic skins

1 Introduction

Wearable electronic devices with light-weight, high performance and mechanical compliance are desired for seamless integration with clothes and human body, realizing diverse applications encompassing smart sensors, electronic skin (e-skin) and health-monitoring gadgets, which also motivated the development of compatible power sources [1-10]. Considering the limited lifetime and pollution problems of traditional batteries that require repetitive charging, triboelectric nanogenerator (TENG) that converts the distributed mechanical energy into electricity based on triboelectrification and electrostatic induction, shows superiorities in wearable applications such as portable power source [11-17], self-powered sensors and e-skin [18-23]. Important progress of textile-based TENGs has been achieved for unobtrusive biomechanical energy harvesting [24-25], as well as continuous, real time, and noninvasive health monitoring [26-29]. Mechanical compliance and stretchability of TENGs exhibit increasing importance for seamlessly integrated wearable applications. Elastic polymers such as polydimethylsiloxane (PDMS) [30-31], silicone rubber [32], ethylene-vinyl acetate (EVA) [33] have been widely utilized for fabrication of stretchable TENG. However, these elastic rubbers are airtight and may cause skin discomfort or even induce inflammation for long-term wearable electronics [34].

In comparison, electrospun membranes with superior breathability, great flexibility, controllable thickness and ease of manufacturability, show great potential for wearable devices [35-39]. Furthermore, electrospinning is capable of producing membranes with micro/nano architectures and high surface rough-

ness, which could effectively improve the contact area and friction effect to enhance the output performance of triboelectric materials [40-42]. A wide range of electrospun nanofibers has been successfully applied to fabricate wearable devices. For example, Li et al. presented an all-fiber based e-skin fabricated with polyvinylidene fluoride (PVDF) nanofibers, carbon nanofibers and polyurethane (PU) nanofibers, while both the triboelectric and electrode layers are non-stretchable [34]. Liang et al reported a stretchable TENG based on polytetrafluoroethylene (PTFE)-PU bilayer membrane and PU-Ag nanowire electrode. However, VHB tapes and a hot-press process are needed for device assembly and the stretchability of the device relies on PU [43]. Some other stretchable electrospun membranes such as PU/carbon nanotubes (CNT)-cellulose nanocrystals (CNC) composites [44], PU-Ag nanowire network [45-46] were also demonstrated as strain sensor or epidermal electrode, in which their deformability also relies on PU. It is challenging to maintain high stretchability as well as strong adhesion between PU and other functional layers, which could affect the deformability and durability of the device. So far, electrospun nanofiber membranes are limited in deformability, in particular the stretchability has been less than satisfactory due to the irreversible sliding of the physically stacked nanofibers, which highly restrains the seamless integration with daily textiles and human body for wearable applications. Although some methods have been attempted to improve the deformability and elasticity of nanofibers materials, such as addition with elastomer [47], decorating with extra coating [48], and thermal crosslinking [49], they suffer from tedious fabrication, reduced air-permeability and high temperature requirement. At present, limited efforts have been channeled onto a one-step strategy at room temperature on the development of nanofiber membranes with intrinsic stretchability in commensurate with highly stretchable electrodes and deformable textiles, which is critical in realizing TENGs with good mechanical compliance for wearable e-textile.

Herein, electrospinning of poly (vinylidene fluoride-co-hexafluoropropylene) (PVDF-HFP) assisted with simultaneous electrospraying of styrene-ethylene-butylene-styrene (SEBS) was performed to fabricate the first breathable nanofibers-membrane with high stretchability and hydrophobicity. The co-deposited SEBS elastomer serves as microsphere-binders among the PVDF-HFP nanofibers, capable of anchoring the nanofibers at distributed location to facilitate reversible fibers sliding upon stretching and therefore enhancing the stretchability. SEBS microspheres also increase hydrophobicity of the PVDF-HFP nanofibers-membrane due to the improvement of surface roughness. The obtained PVDF-HFP/SEBS (PHS) membrane has controllable thickness (from nanometers to microns), high stretchability (ultimate strain of ~490%), great hydrophobicity (static water contact angle (WCA) of ~140°) and breathability (71% of cotton). The stretchable nanofibers-based TENG (SNF-TENG) with effective area of 2 × 2 cm^2 shows output voltage of 85 V and instantaneous power density of 219.66 mW m^{-2}, which is able to power 200 light-emitting diodes (LEDs) array and an electronic watch. The PHS membrane exhibits excellent integrability with stretchable textile, demonstrating multifunctional applications such as self-powered touch or posture sensors, smart raincoat as well as tactile interactive interfaces. The electrospinning-electrospraying integrated technique provides an effective route for fabrication of highly stretchable nanofiber membranes, delivering an attractive feasibility for applying the nanofibers membranes to wearable electronic devices and human-robot interactions.

2 Results and discussion

2.1 Fabrication of self-interlocked stretchable nanofibers based TENG

Block copolymers are known to self-assemble into ordered phase with various periodic nanostructures through electrospinning by selecting suitable solvents, copolymer molecular weight or relative volume frac-

tion between the blocks [50-52]. SEBS is a triblock copolymer of polystyrene (PS) and poly (ethylene butylene) (PEB) with great elasticity, electrospinnability and biocompatibility [52]. PVDF-HFP shows strong electronegativity, hydrophobicity and high chemical stability, which has been widely used as triboelectric layer for TENGs [53-54]. Moreover, electrode with advanced deformability and conductivity is significant to stretchable TENGs considering that robust adhesion among the substrate, electrode and triboelectric layer determines the mechanical durability of the device [55]. Herein, we designed SEBS microspheres by electrospraying with cosolvent system to alter the selective solubility of disparate polymer blocks, forming a self-assembled stretchable SEBS dense membrane with considerable surface roughness (Fig. 1a(I)). A suspension of liquid metal (gallium indium tin (GaInSn), LM) and silver (Ag) flakes in SEBS resin was prepared and deposited onto the SEBS membrane by screen printing (Fig. 1a(II)) to prepare the stretchable conductor. The strategy shows merits of stretchability, conductivity and seamless integratability with the substrate. The resultant conductive SEBS membrane was used as the collector during PVDF-HFP electrospinning as shown in Fig. 1a(III). The electrospraying was performed simultaneously to deposit SEBS elastic microspheres as binders to interlock the electrospun PVDF-HFP nanofibers, generating a PHS membrane with high stretchability, breathability and waterproofness on the electrode.

A sandwiched SNF-TENG was assembled as shown in Fig. 1b, three layers are tightly adhered to each other due to the in-situ interlocking deposition technique (Fig. 1c), ensuring a 175 μm thick SNF-TENG with good deformability and durability. PHS nanofibers-membrane serves as the triboelectric layer. SEM image at top right of Fig. 1c reveals that PVDF-HFP nanofibers were well locked by the SEBS microspheres, providing stable hierarchical/interlocked architectures with distinct rough surface. Importantly, such an interlocked structure exerted on the PVDF-HFP nanofibers could effectively adjust the tensile stress distribution with the

help of soft elastomeric SEBS that buffers the stress by absorbing more energy at strain state, endowing the PHS membrane with high stretchability and deformability. The elastic conductor also exhibited a significant role that enables the seamless integration between different functional layers of SNF-TENG. The perfect fusion of the elastic conductor and substrate layer can be achieved thanks to the utilization of the same polymer matrix-SEBS. The printable elastic conductor ink with toluene as solvent will slightly dissolve the SEBS substrate during the screen-printing process, resulting in an embedded interface with tight adhesion between them. As the mixed solvent of 85% mesitylene/15% N,N-Dimethylformamide (DMF) for electrospraying has high boiling temperature (about 160℃) that could not dried quickly, the subsequently electrosprayed SEBS microspheres landed on the conductive SEBS film (Fig.1a (III)) will inevitably carry little residual solvent that could slightly etch the SEBS matrix in conductor. Meanwhile, the SEBS microspheres serve as binder to interlock the PVDF-HFP nanofibers network, enabling the tight mechanically merging between the triboelectric layer and electrode. Therefore, commendable integration between substrate, electrode and PHS layers can be achieved thanks to the utilization of SEBS binder, which guarantees the mechanical stability of the SNF-TENG even at strain of ~125% (Fig. S1). The device shows great recovery upon tensile loading-unloading cyclic test (125% strain), indicating high energy dissipation enabled by the stretchable PHS membrane (Fig. 1d). Slight residual strain (~21%) was observed for the first unloading cycle, owing to the inherent thermoplasticity of PVDF-HPF in which energy was dissipated for the polymer chains disentanglement. Ultimately, the SNF-TENG possesses great flexibility, stretchability, hydrophobicity and washability (Fig. 1e-g), bringing promises for wearable applications.

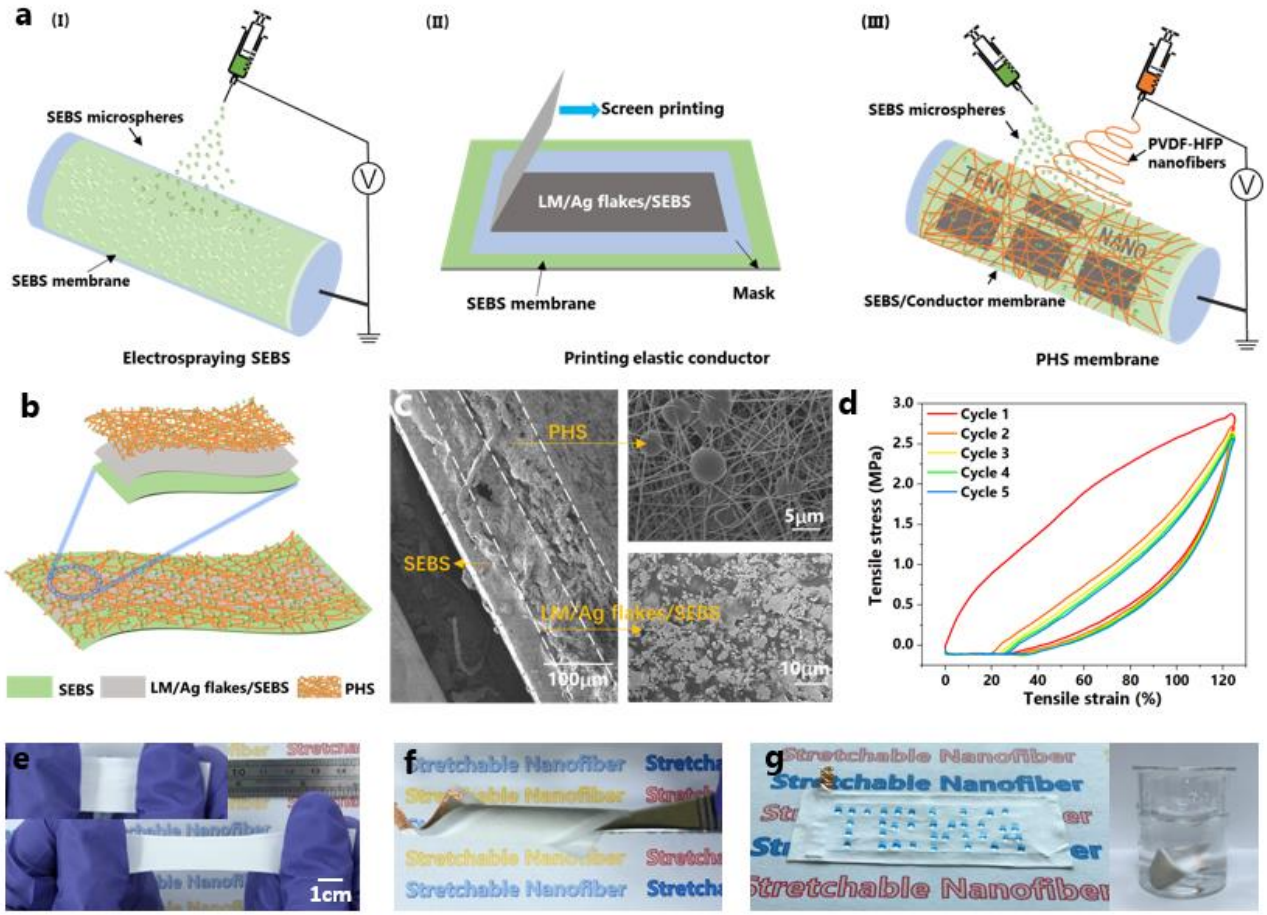

Fig. 1. Structure and properties of self-interlocked stretchable nanofiber based TENG (SNF-TENG). (a) Schematic illustration of the fabrication process of the SNF-TENG. (i) Electrospraying to assemble SEBS membrane, (ii) Screen printing of stretchable electrode on SEBS membrane, (iii) Simultaneous deposition of PVDF nanofibers and SEBS microspheres on the conductive SEBS membrane. Electrode pattern shows the feasibility of this in-situ deposition and assembly technology to fabricate SNF-TENGs with desirable geometrics. (b) Structure of the designed SNF-TENG with sandwich-like architecture. (c) Cross-sectional SEM image and surface morphology of the SNF-TENG. (d) Cyclic tensile properties of PHS based SNF-TENG. (e-g) Photographs demonstrating the stretchability, flexibility, hydrophobicity and washability of SNF-TENG.

The same method is also adopted for textile-TENG fabrication by replacing the SEBS substrate to knitted polyethylene terephthalate (PET) or other highly stretchable textiles, indicating the advantages of this integrated technology by screen printing of elastic conductor and in-situ deposition of stretchable nanofibers

triboelectric layers that could achieve seamless integration of functional stretchable nanofibers and fabrics.

2.2 Stretchability, hydrophobicity, and breathability of PHS membrane

As the properties of PHS membrane highly rely on the content of PVDF-HFP and SEBS, a series of PHS membranes with different weight ratios of PVDF-HFP/SEBS were fabricated by controlling the feeding rate of polymer solutions through simultaneously electrospinning and electrospraying (Fig. S2). SEM images in Fig. S3 show the composite membranes comprising of PVDF-HFP nanofibers embedded with different amount of SEBS microspheres. FTIR reveals that there is no additional chemical bonding formation between the two components, therefore it is conjectured that the PHS membranes were physically interlocked rather than chemical interaction (Fig. S4).

Normally, PVDF-HFP nanofiber membranes are prone to delamination upon contacting with other materials due to the weak adhesion between the stacked nanofiber layers, resulting in poor mechanical stability [34]. In comparison, the PHS membrane with the same thickness as the PVDF-HFP nanofiber membrane exhibited no delamination between nanofibers after continuous vertical contact-separation with aluminum film or air flow blown (Fig. S5). Its robust structure stability is due to the interlayer locking between PVDF-HFP nanofibers and SEBS microspheres, which was verified by the cross-section SEM observation shown in Fig. S6. The effect of the amount of SEBS microspheres on the tensile properties of PHS membranes are given in Fig. S7. The elongation at break of the PHS membranes was enhanced with increasing SEBS content. PHS membrane with the weight ratio (PVDF-HFP: SEBS) 1:9, 3:7, 5:5 can sustain tensile strains of 1400%, 490% and 304% respectively, which are higher than that of pure PVDF-HFP nanofibers membrane (~270%). In addition, the Young' modulus values decrease with the increase of SEBS content in the PHS membranes (Tab. S1). All the PHS membranes demonstrate lower Young' modulus than that of

PVDF-HFP. This confirms that the addition of SEBS microspheres delivers better softness to the PHS membrane, which will effectively dissipate the energy upon deformation. A higher tensile strain for 30%PVDF-HFP/ 70%SEBS membrane (~490%) than that of PVDF-HFP nanofibers membrane (270%) can be shown in Fig. 2a. Thus, it is evident that the interlocked networks of PVDF-HFP nanofiber by SEBS microspheres could effectively enhance the stability, stretchability and deformability of PHS membrane.

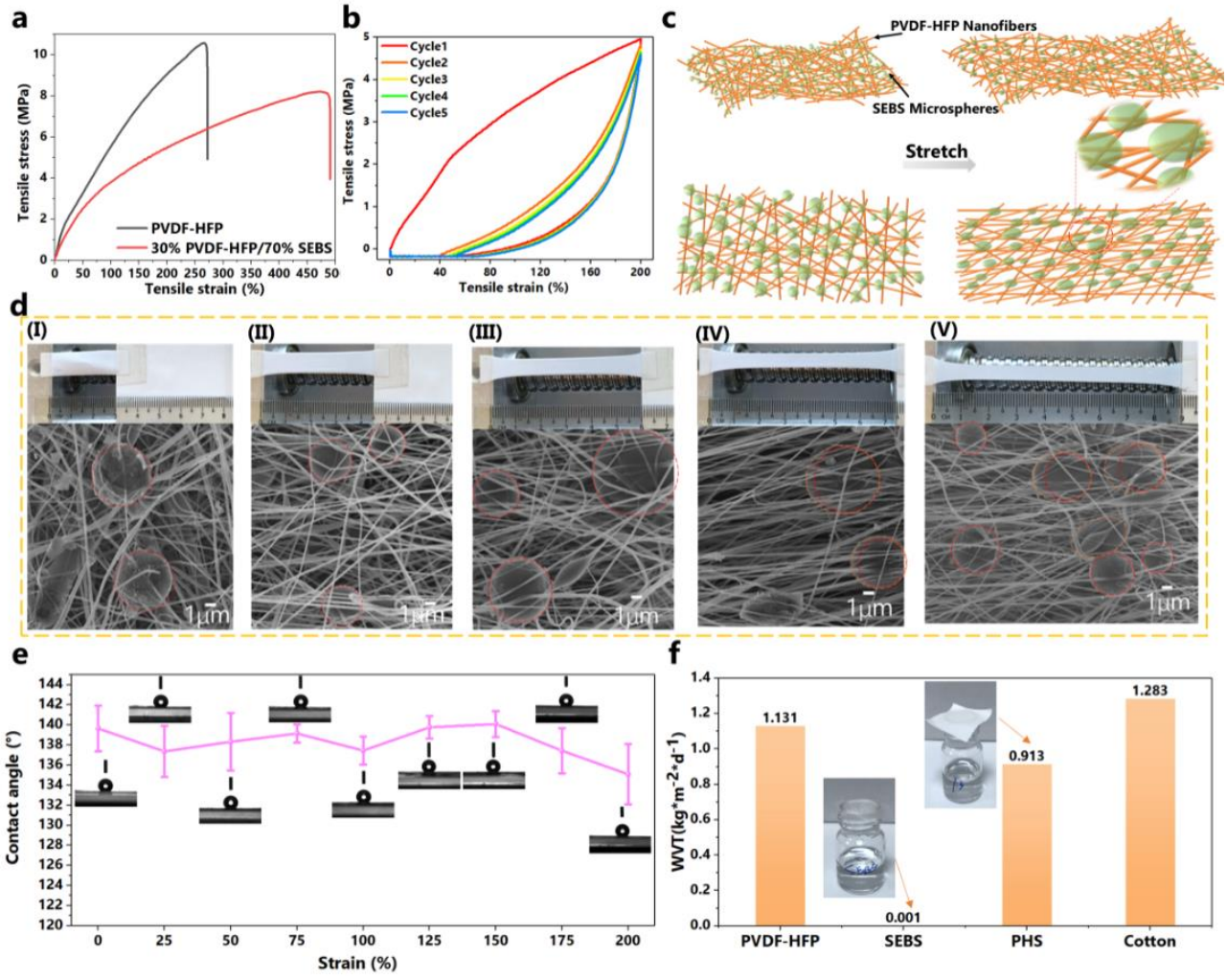

Fig. 2. Properties of the PHS membrane. (a) Tensile stress-strain curves of the pure PVDF-HFP and PHS (30% PVDF-HFP, 70% SEBS) membrane. (b) Cyclic tensile stress-strain curve of PHS membrane (30% PVDF-HFP, 70% SEBS). (c) Schematic of the stretchable mechanism of PHS membrane. The orange line represents PVDF-HFP nanofiber and the light green circle or ellipse represents SEBS microspheres. (d) Photograph and SEM images of the PHS membrane (30% PVDF-HFP, 70% SEBS) at (I) 0%, (II) 50%, (III)

100%, (IV) 150% and (V) 200% strain. (e) Static water contact angle (WCA) of PHS membrane (30% PVDF-HFP, 70% SEBS) at different strain. (f) Water vapor transmittance (WVT) rates of the PVDF-HFP, SEBS, PHS membrane (30% PVDF-HFP, 70% SEBS) and cotton.

Meanwhile, the desired balance between tensile properties and triboelectric performance is a key parameter for SNF-TENG. According to Fig. S8, output voltage of devices based on the PHS membranes with higher PVDF-HFP content exhibit higher values at the same condition. The PHS membranes with the PVDF-HFP/SEBS weight ratio of 1:9, 3:7, 5:5 show output voltage of 33 V, 93 V and 131 V respectively, which is 24%, 70% and 97% that of pure PVDF-HFP (135 V). The reducing voltage output of the PHS membranes with higher SEBS weight ratio could be ascribed to the lower triboelectric affinity of SEBS compared to PVDF-HFP. Having too much SEBS microspheres (>90%) with tiny PVDF-HFP nanofibers could not attain a hierarchical structure with higher roughness as most of the PVDF-HFP nanofibers were covered by the aggregation of SEBS (as shown in Fig. S3). Considering both stretchability and triboelectric performances, we selected 3:7 (PVDF-HFP: SEBS) as the optimal weight ratio for PHS membrane fabrication. Further mechanical performance tests were conducted (as shown in Fig. S9). The PHS membrane (30% PVDF-HFP/70% SEBS) shows increased residual strain (7.5% ~ 40%) mainly at the first loading-unloading cycle when the tensile strains increased from 50%, 100%, 150% to 200%. It suggests that partial physical displacement occurred between nanofibers, together with loss of strain energy in the form of irrecoverable heat energy as generated by the sliding of PVDF-HFP thermoplastic molecule chains over each other [56-57]. Thereafter, lower tensile stresses were attained and PHS membrane showed favorable recovery even by applying 200% tensile strain for 5 cycles (Fig. 2b). It indicates the movement of polymeric molecule chains reached a relative stable condition due to the constraint of elastomeric SEBS microspheres. Tensile strain of 100% was applied on the PHS membrane at different strain rates (50-150 mm min^{-1}), which verified that no

obvious impact on the recoverability of material (Fig. S10). From the digital photos taken, there are no visible damages observed on the PHS membrane at strain of ~200% (Fig. S11). It indicates that PVDF-HFP nanofibers membrane could recover well upon cyclic stretching, performing as an elastic membrane.

The stretchability mechanism of PHS membrane can be schematically explained (as shown in Fig. 2c). The PHS membrane consists of SEBS microspheres randomly embedded within the curly PVDF-HFP nanofibers (Fig. 2d (I)). Once the membrane is stretched (~50%), the random PVDF-HFP nanofibers are tightened along the stretching direction firstly (Fig. 2d(II)), sustaining most of the tension distributed within and on the surface of the PHS. The realignment is almost an irrecoverable process, generally leading to residual strain. As the strain increases to 100%, PVDF-HFP nanofibers are further tightened (Fig. 2d (III)) and the displacement begins to be increasingly restrained by the embedded SEBS microspheres. When further increasing the strain to 150% and 200%, apparent deformation was observed on the SEBS microspheres, which was induced by the increasing displacement between nanofibers that have been fully tightened (Fig. 2d (IV)) and partial fibers were being damaged due to the over loading (Fig. 2d (V)). In addition, the existence of SEBS microspheres with circular shapes at 200% strain is due to the stress mostly concentrated on the PVDF-HFP nanofibers, suggesting that only partial SEBS microspheres are subjected to the tensile stress at 200% strain. Therefore, higher breaking elongation of ~490% can be achieved (Fig. 2a). During the stretching processes, SEBS microspheres play an important role as the binder to effectively limit the physical sliding of PVDF-HFP nanofibers. The elastic network constructed by SEBS microspheres is capable of dissipating the tensile stress to well recover the stretched nanofibers membrane in shape. Therefore, the PHS membrane with structure of co-deposited nanofibers and elastic microspheres shows superior stretchability than that of the commonly fabricated electrospun nanofibers [35-37].

The hierarchical network of nanofibers and microspheres also bring superior waterproofness to the PHS membrane. As shown in Fig. S12, electrosprayed SEBS and electrospun PVDF-HFP membranes are both intrinsic water-resistant materials with the static WCA of 103° and 132°. PHS membranes with PVDF-HFP weight content higher than 20% all have an apparent WCA of around 140°, which could be mainly ascribed to the SEBS microspheres that roughened the surface (Fig. S3), enabling trapped air in the pores with outward pressure to resist the penetration of water droplet [58]. The surface wettability is determined cooperatively by its morphology (surface roughness) and intrinsic material properties (surface energy) [59]. The hydrophobic surface can be obtained by directly electrospinning a hydrophobic polymer or modifying the rough surface with a low-surface-energy material [60]. Herein, the PHS membranes with 50-80% content of SEBS microspheres show comparable WCAs around 140° (Fig. S12), indicating 50% content of SEBS microspheres embedded into the PVDF-HFP nanofibers is enough to construct a favorable micro-nano hierarchical structure with enhanced hydrophobicity. Further increasing the SEBS content could not improve the WCA, but endowing PHS membrane with higher stretchability. The self-interlocked hierarchical architectures ensure the stable hydrophobicity of the PHS membrane even upon stretching up to ~150%. Slight decreased WCA was observed on a typical PHS membrane (30% PVDF-HFP/ 70%SEBS) with tensile strain higher than 150% (Fig. 2e), which is due to the increased capillary effect of aligned nanofibers upon higher stretching. The stable WCA suggests there is no large change in the surface roughness of the PHS membrane upon stretching, which is of significance to maintain the triboelectric properties under extreme stretching conditions.

Additionally, considerable air permeability is attainable owing to the favorable porosity of PHS membranes. Normally, the air permeability could be evaluated by the Fickian diffusion of water vapor through the

porous structure, which is driven by the relative humidity between two sides [34, 61]. Thus, water vapor transmittance (WVT) rate was applied here to explore the breathability of PHS membranes. The samples were covered on bottles contained water to monitor the weight change of the setup, normalizing as WVT. Fig. 2f shows that the WVT of the 3:7 PHS membrane reaches 80% of PVDF-HFP, 71% of cotton and no water droplets accumulation can be found at its inner surface (Fig. S13). Overall, the in-situ deposited SEBS microspheres act as elastomeric binders and hydrophobic modifiers for enhancing the deformability and waterproofness of PVDF-HFP, endowing the higher stretchability, hydrophobicity, breathability and triboelectric performance to the composite membrane. These compelling features render the self-interlocked stretchable PHS membrane highly desirable for wearable triboelectric devices.

2.3 Energy harvesting performance of SNF-TENG

Admittedly, flexible and stretchable electrode is an essential component for TENGs and the mechanical durability among different functional layers needs to be addressed. Printable elastic conductor consists of conductive fillers and polymer matrices s with great conductivity, stretchability, substrate adaptability and durability, is promising for wearable devices [62]. Here, we synthesized LM-Ag flakes-SEBS elastic conductor (relevant details can be found in Fig. S14 and experimental section) using as stretchable electrode for SNF-TENG. The elastic conductor is capable of being screen printed on the SEBS substrate with different geometric forms, such as rectangle or the "NANO" letter (Fig. 3a). Tight adhesion among substrate, electrode and PHS membrane was successfully achieved (verified by the cross-sectional SEM image given in Fig. 1c) thanks to the matched Young's modulus of different layers with the utilization of SEBS binder by in-situ deposition technology. The elastic conductor printed on the SEBS substrate clearly displayed excellent conductivity and a low resistance about 3 Ω can be maintained even at 200% strain (Fig. 3b), which is as-

cribed to the GaInSn that can be released to reestablish the electrical interconnects between the Ag flakes as shown in Fig. S15. Here, the GaInSn LM particles provide dynamic and robust electrical anchors between the conductive fillers. Mechanical robustness of the electrode was also investigated by monitoring the resistance during fatigue cycles at 150% strain. Although the resistance slightly increases, its value is still lower than 7 Ω after 2000 cyclic tests (Fig. 3c). The change is negligible for output performance owing to the large impendence of TENGs [63].

The mechanical energy harvesting mechanism of the SNF-TENG can be explained as shown in Fig. 3d. The electricity generation originates from contact electrification and electrostatic induction [64-65]. Firstly, when the alien surface (aluminum or skin) contacts with the PHS membrane, electrification occurs owing to the charge transfer between them. The net negative static charges are generated on the PHS membrane due to its higher surface electron affinity. Once the two surfaces are separated to a certain distance, an electrical potential difference (voltage) is built and the negative charge on the PHS membrane induces positive charge to the electrode. Free electrons flow from the electrode to ground, generating the current pulse. The electrostatic equilibrium is achieved once the alien surface and PHS membrane reaches the maximum displacement. As the alien surface moves to the PHS membrane again, the induced positive charges in the electrode decreases (the electrons flow back to the electrode) and a reversed output signal generates. The continuous contact-separation process will generate voltage and current pulse, converting mechanical energy to electricity.

The output performance of SNF-TENG (2 × 2 cm^2 area) under different tensile strain conditions was investigated by applying tapping force of 30 N at 5 Hz (Fig. 3e). The output voltage (V_C), short-circuit current (I_{SC}), transferred charge (Q) of the device show an increase trend with tensile strain (Fig. S16). The V_C

of 85 V, I_{SC} of 4 μA, Q of 15 nC can be detected at 0% strain and their value reaches 160 V, 7 μA, 29 nC at 100% strain. The increase of output performance is attributed to the variations of contact area at strain state. The output performance of SNF-TENG under different applied forces, contact frequencies were also investigated. The device shows a V_C of ~ 60 V at 5 N, indicating it could be easily triggered (Fig. 3f and Fig. S17). The V_C, I_{SC} and Q show a mild increase trend with contact frequency lower than 8 Hz, and commence a reduction when the contact frequency is higher than 10 Hz (Fig. S18). The lower output voltage at 2 Hz and 14 Hz were attributed to the insufficient charge transfer due to long separation or transient contact. The power output performance of SNF-TENG was evaluated by varying different external load resistors. As shown in Fig. 3g and Fig. S19, the output voltage of SNF-TENG gradually increases from 2.88 V to 73.28 V as the external load changes from 500 kΩ to 150 MΩ. The output current shows decreasing trend with the increase of load resistance. The extracted maximum instantaneous peak power density of 219.66 mW m^{-2} is achieved at a matched resistance of 20 MΩ. Moreover, the durability test for the SNF-TENG was conducted by continuous contact-separation at the frequency of 5 Hz. It can be seen from Fig. 3h that there is no visible change of the output voltage after long period of continuous operation for 3000 s (15000 cycles). These properties present the promising potential of SNF-TENG for practical applications.

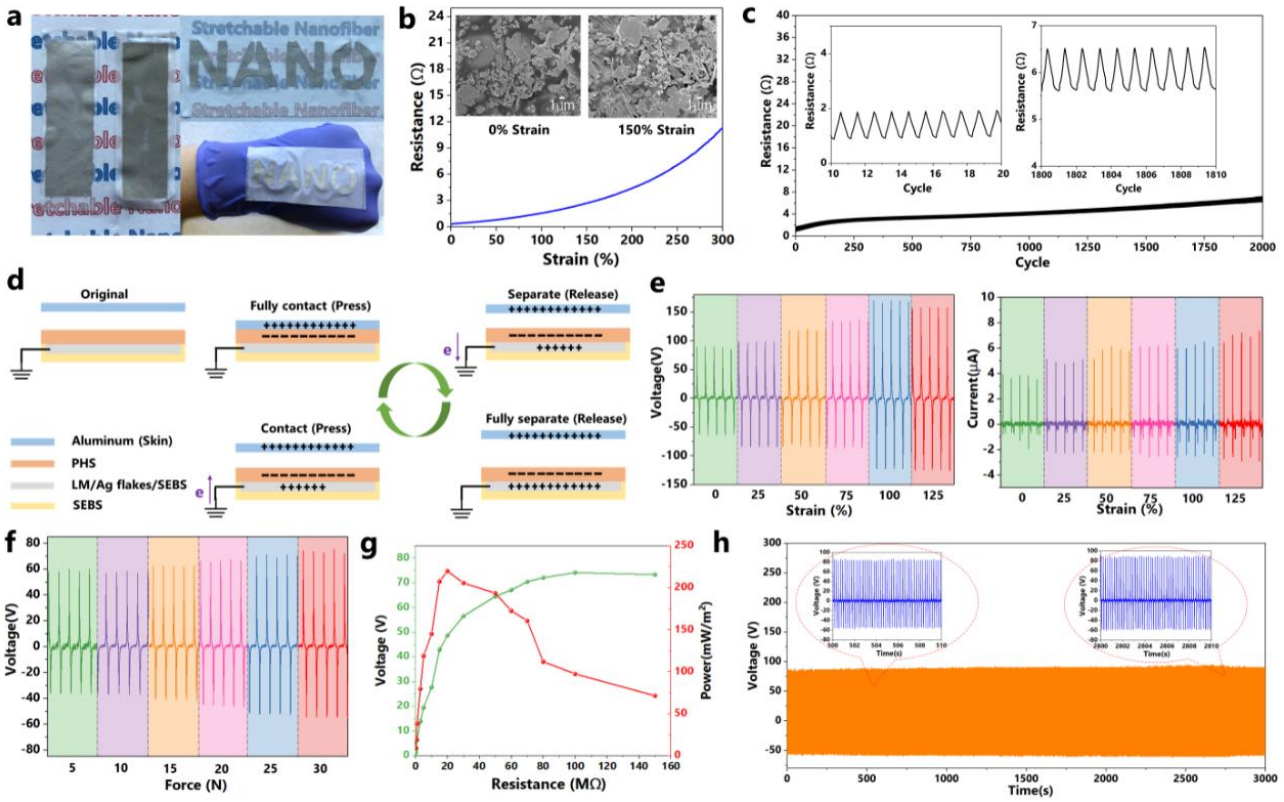

Fig. 3. Elastic conductor properties and triboelectric performance of SNF-TENG. (a) Demonstration of the flexibility of the elastic conductor. (b) Resistance-tensile strain curve of the elastic conductor printed on the SEBS substrate. (c) Demonstration of stable resistance of the elastic conductor under 2000 cycles of 150% tensile strain. (d) Working mechanism of the SNF-TENG. (e) Output performance of the SNF-TENG under different tensile strain state. (f) Output performance of the SNF-TENG under different applied force. (g) Dependence of voltage and instantaneous peak power density of the SNF-TENG under different resistance load conditions ($P = I^2R$). (h) Output durability of the SNF-TENG under continuous measurement.

The inherent waterproof properties of SEBS and PHS membranes render the promising application of SNF-TENG in water environment. Here we demonstrated the SNF-TENG that is capable of harvesting water energy with high output and remarkable robustness. The working mechanism of liquid-solid triboelectrification shown in Fig. 4a is similar to that of mechanical energy harvesting, which relies on the contact electrification and electrostatic induction process between water droplets and PHS membrane. The hydrophobic surface allows water droplets to slide away quickly and avoid the formation of residual liquid film,

which enables complete charge transfer in each cycle and ensures the high output performance of the device. The output performance of a SNF-TENG with area of 3 × 3 cm^2 was investigated under flowing water. The output voltage and current increase with the water speed in the range of 4.03-11.33 ml s^{-1} and then decreases (Fig. S20). The highest V_C, I_{SC} reaches 65 V and 16 μA at the speed of 11.33 ml s^{-1}. In addition, we found that the optimal device-vertical angle (defined as the angle between device and the vertical direction) is around 30°-45° (as shown in Fig. S21-22). The lower device-vertical angle results in insufficient contact between water droplets and PHS membrane, while higher value will generate residual liquid film on the device surface, screening the charge generation and suppressing the complete electron transfer in each cycle.

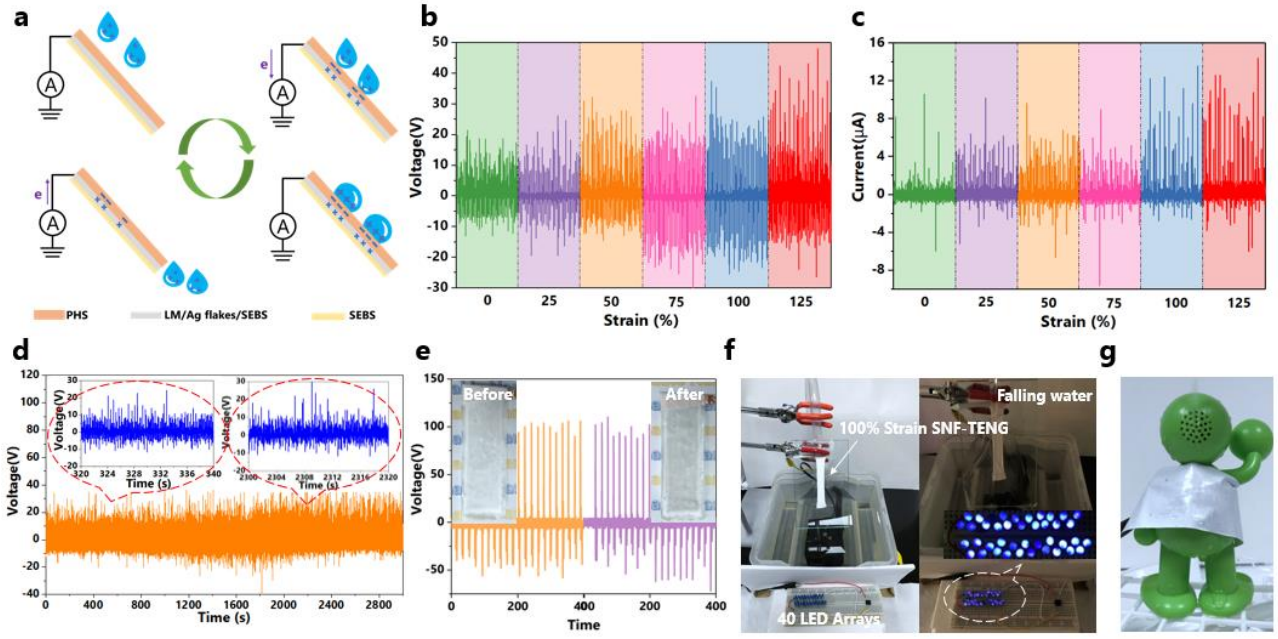

Fig. 4. Performance of the SNF-TENG under water driven mode. (a) Water energy harvesting mechanism of the SNF-TENG. (b-c) Output performance of the SNF-TENG for water energy harvesting under tensile strain conditions. (d) Output durability of the SNF-TENG. (e) Output performance of the SNF-TENG before and after extended washing of 15 h. (f) Demonstration of the SNF-TENG that drives 40 LED arrays under water flow at 100% strain. (g) Demonstration of the smart raincoat for electricity generation.

The performance of the water driven SNF-TENG under different tensile strain states was also investi-

gated, as shown in Fig. 4b-c. The output voltage achieves approximately 45 V at 125% strain (higher than that of 20 V at 0% strain), which is mainly ascribed to the effective area increase of the device at strain state. The great durability of SNF-TENG delivers a water energy harvester with reliable output for continuous working (Fig. 4d). The output voltage of the SNF-TENG that underwent 15 h washing still remains stable, suggesting an admirable robustness of the device (Fig. 4e). Moreover, the SNF-TENG (1.5 × 4.5 cm^2 area, Fig. S23) could easily power 40 LED arrays without batteries by water flow at 100% tensile strain state (Fig. 4f, Supplementary Video S1). The SNF-TENG is also capable of working as wearable raincoat based on a device with the letter "TENG" patterned electrode (Fig. S24), which shows a stable output voltage of 24 V under 8.4 ml s^{-1} flowing water (Fig. 4g). Benefiting from the customizable electrode and self-assemble PHS membrane, it is easy to employ other complex substrates to fabricate wearable smart raincoats.

2.4 SNF-TENG for power sources and self-powered sensing

The self-interlocked stretchable PHS based SNF-TENG demonstrates multiple application potentials. Firstly, the SNF-TENG can scavenge mechanical energy of human motions. As demonstrated in Fig. 5a and Supplementary Video S2, 200 LED arrays could be easily lighted up when tapping a SNF-TENG (4.5 × 4.5 cm^2 area) with hand both at 0% and 50% strain (Fig. S25). The generated electricity can be collected and stored to power different portable electronics based on the equivalent circuit shown in Fig. 5b, wherein the rectifier bridge and capacitor are utilized to alternate the SNF-TENG outputs and store the electricity, respectively. Various capacitors (22-100 μF) can be charged by the SNF-TENG (4.5 × 4.5 cm^2 area) to meet different application requirements (Fig. S26). Fig. 5c depicts the real-time charging curve of a 33 μF capacitor driven by the SNF-TENG. The capacitor voltage reached 1.43 V within 140 s by hand tapping the device and the voltage-step curve for the charging process is apparent (inset of Fig. 5c). The stored electricity in the

capacitor is able to power a wearable electronic watch without battery, the discharging curve of the capacitor was also given. The SNF-TENG could be attached to a variety of objects surface and serve as power source thanks to its flexibility, stretchability and shape adaptability (Fig. 5d).

Given the great mechanical adaptability of PHS membrane, the SNF-TENG can be utilized as self-powered e-skin. As an exemplification, the SNF-TENG (1.5 × 4.5 cm^2 area) was attached on a finger or worn on a finger joint and the characteristic output signals were detected by cyclic finger bending. When the e-skin is attached on the finger, the positive and negative output signal shows similar value (~12.5 V), which may attribute to the comparable contact-separation amplitude between the e-skin and finger (Fig. 5e I, Supplementary Video S3). However, the e-skin that worn on a finger joint works in the bending mode generates different waveform signals (Fig. 5e II, Supplementary Video S3). The amplitude of the negative output voltage value (~6 V) is higher than the positive one (~3 V), owing to the deformation degree of the e-skin during the bending process is higher than the straighten process. Furthermore, the e-skin could be worn on multiple fingers to reveal complex motions. The synchronous in-phase signal of the e-skins worn on the index finger and middle finger joints can be detected when grabbing and releasing a bottle by hand (Fig. 5e III and Supplementary Video S4). And the synchronous out-of-phase signal could also be measured when the index finger and middle finger bend alternately (Fig. 5e IV and Supplementary Video S4). Thereupon, this e-skin shows a promising smart application such as self-powered feedback sensors in robots, remote controllers as well as continuous healthcare monitoring in real-time.

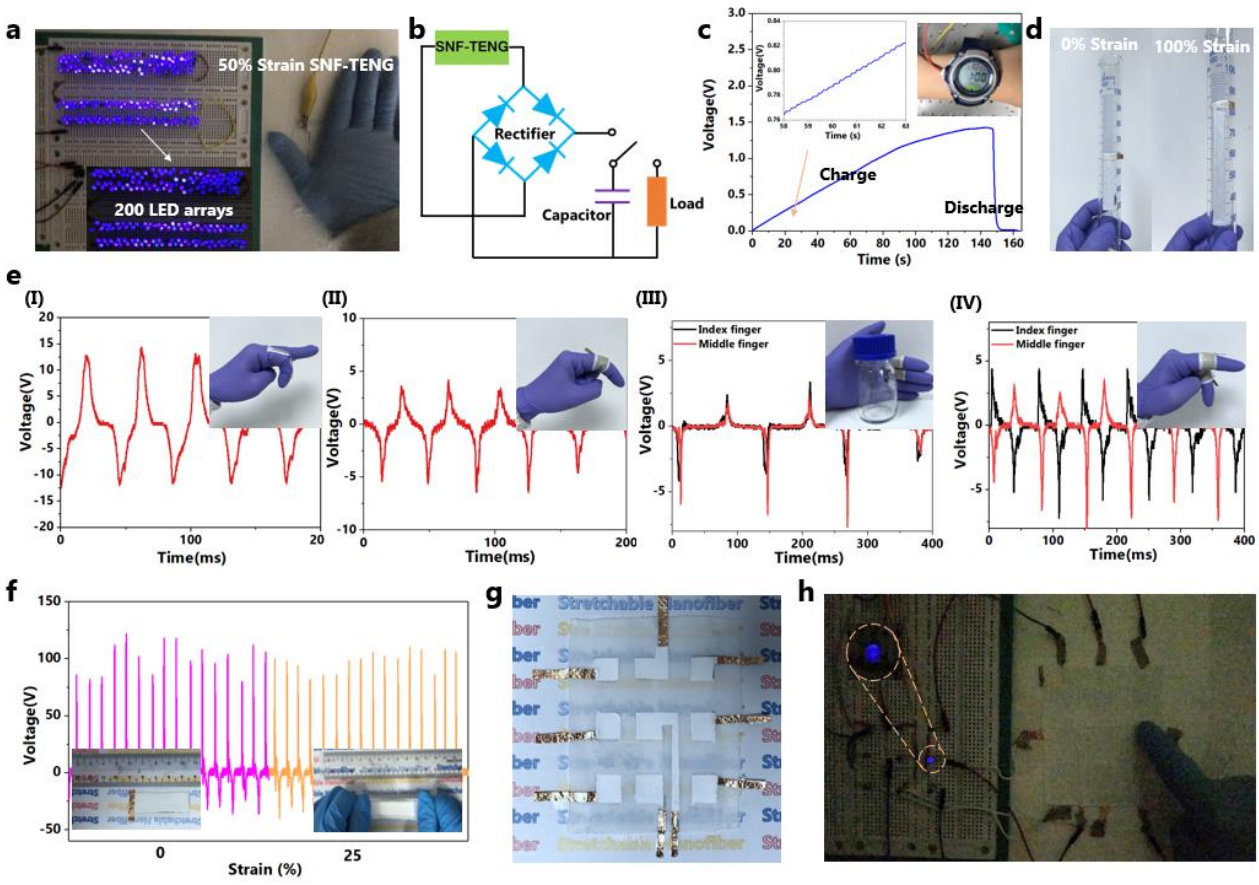

Fig. 5. SNF-TENG and textile-TENG work as power sources or sensors. (a) SNF-TENG drives (4.5 × 4.5 cm^2) 200 LED arrays by tapping. (b) Circuit diagram for SNF-TENG works as power source for electronic device. (c) SNF-TENG as power sources to charge a 33 μF capacitor for powering an electronic watch. (d) Stretchability demonstration of the SNF-TENG. (e) The characteristic output signal of the SNF-TENG (1.5 × 4.5 cm^2) under different finger motions. (f) Output performance of textile-TENG (1.5 × 4.5 cm^2) at 0% and 25% strain. (g-h) Demonstration of textile-TENG based tactile interactive interface that is able to map different touch events.

Considering textile is an ideal substrate with excellent deformability, breathability and compatibility for incorporation with our daily clothes [26-27]. The printable elastic conductor with great adaptability to different substrates provides possibility for seamless integration of deformable textile and PHS membrane to fabricate a stretchable, wearable textile-TENG. Herein, the knitted PET textile based TENG with great tensile recovery capability after cyclic stretching was successfully assembled (as demonstrated in

Supplementary Video S5). The excellent interlayer adhesion among the elastic conductor, PHS membrane and PET textile can be achieved owing to the in-situ self-interlocked fabrication process as well as the binder enhancement of SEBS. The output performance of the textile-TENG (1.5 × 4.5 cm^2 area) driven by hand tapping keeps stable (around 125 V) at 0% and 25% strain, verifying the durability of device (as shown Fig. 5f and Supplementary Video S6). And the textile-TENG integrated on the cloth also exhibits favorable triboelectric outputs (Fig. S27). Owing to the linear response output of the textile-TENG at different pressure, it can be applied as tactile sensor with the detected sensitivity of 0.68V kPa^{-1} in the pressure range of 8-89 kPa and response time of 3.14 ms by finger tapping (as shown in Fig. S28-29). Furthermore, we fabricated a textile based tactile interactive interface embedded with 9 touch sensor unit (1 × 1 cm^2 area) and connected it to 9 LEDs (Fig. 5g). The textile based tactile interactive interface is able to map the finger touch behavior in a real time by lighting corresponding LED without any power supply (Fig. 5h and Supplementary Video S7), showing a wearable interface with great potential for self-powered security or interactive entertainment system.

3 Conclusions

In summary, we accomplish a self-interlocked stretchable, hydrophobic and breathable nanofiber membrane derived from an innovative strategy of simultaneously electrospinning and electrospraying. The in-situ deposited SEBS microspheres act as elastic binder and hydrophobic modifier, realizing a stretchable nanofibers-based membrane with favorable waterproofness and breathability. Moreover, the PHS based SNF-TENG and textile-TENG demonstrated multifunctional and wearable potentials with great mechanical transformability, high durability as well as exceptional energy harvesting capabilities from human motions and water flow. It can drive 200 LEDs and an electronic watch easily by hand tapping as well as utilize as

smart raincoat, self-powered e-skin, real-time human motion sensor and tactile interactive interface in harsh conditions. The development of stretchable nanofiber membrane with high hydrophobicity and breathability will open new avenues for self-powered e-skin, biological behavior sensors and wearable electronic devices.

4 Experimental sections

4.1 Fabrication of PHS membranes

PHS membranes were fabricated by electrospinning of PVDF-HFP and electrospraying of SEBS simultaneously. Briefly, SEBS (S/EB weight ratio 20/80, Tuftec™ H1052) was dissolved in the Mesitylene/ N,N-Dimethylformamide (DMF) mixture solvent (85 %v/15 %v) by stirring (400 rpm) at 60 ℃ for 12 h to prepare 12 wt % homogeneous solution considering that mesitylene could dissolve both PS and PEB blocks, while DMF is a good solvent for the PS block only [49-50]. PVDF-HFP (Sigma-Aldrich, M_w ~ 455,000) pellets were dispersed in DMF/Acetone (60 %v/40 %v) mixture solvent by stirring (400 rpm) at room temperature for 6 h to obtain 12 wt% homogeneous solution. All PHS membranes were fabricated by synchronous electrospinning of PVDF-HFP and electrospraying of SEBS under the applied voltage of 20 kV. The weight ratio of the PVDF-HFP and SEBS was adjusted by controlling the solution feed rate (controlled by the by syringe pump), as shown in Tab. S2. Typically, the solution feed rate for the 3:7 PHS membrane is set to 0.9 ml h^{-1} for PVDF-HFP solution and 2.1 ml h^{-1} for SEBS solution. The distance between aluminum foil collector and nozzles was set to 15 cm. A heating unit with the power about 400 W was used to promote solvent evaporation during the electrospinning (conducted at 70 ± 3% humidity and 23 ± 2°C). All the obtained membranes were dried at 60 °C for 2 h to remove the residual solvents.

4.2 Fabrication of LM-Ag flakes based elastic conductor

The GaInSn alloy (62% Ga, 25% In, 13% Sn, Melting point: 5 °C) and Ag flakes (Sigma-Aldrich, 10 μm) were used to prepare the elastic conductor. Briefly, 1.5 g GaInSn alloy was added with 6 ml toluene. The GaInSn LM in toluene was sonicated for 30 min in an MRC AC-200H sonicator with the power of 100 W. Then the solution was stand for 30 min to precipitate liquid metal particles (as shown in Fig. S14). This is followed by adding 1.5 g Ag flakes and 0.7 g SEBS resin (40 wt %), then mixing to obtain the LM-Ag flakes-SEBS elastic conductor.

4.3 Fabrication of the PHS based TENG

Firstly, the PHS membrane based TENG was fabricated. The membrane with the 2 × 2 cm^2 area was fixed to a conductive double-sided tape at which the other side was pasted to the center of a commercial PET film (2.5 × 6 cm^2 area). The other conductive double-sided tape with one side pasted to an aluminum foil (2 × 2 cm^2 area) was affixed to another PET film (2.5 × 6 cm^2 area). Then the wider side edges of the two PET films was pasted by a VHB tape as spacers with the thickness of 2 mm to assemble the TENG.

For the SNF-TENG and textile-TENG, the LM-Ag flakes elastic conductor was firstly printed on the electrosprayed SEBS membrane or knitted PET textile using the homemade mask. Then the printed conductive SEBS substrate was dried at 60 °C for 15 min. Finally, the conductive SEBS membrane was affixed to the collector (electrode upwards) and the synchronous electrospinning of PVDF-HFP and electrospraying of SEBS were conducted to assemble the devices.

4.4 Characterization and electrical measurement

The morphology of the PHS membranes, LM-Ag flakes-SEBS conductor and the device were charac-

terized by a field-emission SEM (FE-SEM, JEOL 6340F). The infrared spectral characteristics of the membranes were measured using Fourier Transform Infrared (FTIR) spectrometer (PerkinElmer, Frontier). The static water contact angle was tested by contact angle measuring system (Dataphysics OCA15 Pro) with the droplets of 5 μL. Tensile strain tests for the membranes were conducted by Static Mechanical Tester (Instron, 5567). The sample was cut to the dumbbell shape following the ASTM D638 specimen dimensions (Type V), as shown in Fig. S30. The resistances of the elastic conductor were measured using a Keithley 2400 source meter. The customized system which consists of an amplifier (SINOCERA YE5871A), a function generator (Agilent 33220A) and an electromechanical vibrator (SINOCERA JZK-10) is applied to evaluate the performance of the as made TENGs. The force transducer (SINOCERA CL-YD-331), oscilloscope (Tektronix MDO3024, impedance = 100 MΩ), low-noise current preamplifier (SR570, impedance = 4 Ω, Stanford Research Systems) and programmable electrometer (Keithley 6514, Tektronix Inc., USA) were used to measure the applied force, output voltage, short-circuit current and transferred charge. The water speed was controlled by a peristaltic pump (BT100-2J). All the electrical measurements were conducted in ambient environment (Temperature 23 ± 2 °C; RH, 70% ± 3%). The experiments involving human subject have been performed with the full, informed consent of the volunteer and approved by the university (ref. no. IRB-2017-08-038).

Acknowledgements

The current work is supported by the NRF Investigatorship (NRF-NRFI2016-05) under the National Research Foundation, Prime Minister's Office, Singapore. The authors (Y. Li and X. Zhang) also thank the support from China Scholarship Council (Grant No. 201906270122).

Author Contributions

Yi Li and Jiaqing Xiong contributed equally to this work. Yi Li, Jiaqing Xiong, and Pooi See Lee conceived the idea and wrote the paper. Yi Li and Jiaqing Xiong designed the scheme, fabricated the membranes and devices, conducted materials characterization and analyzed the data. Jian Lv helped to prepare the elastic conductor. Yi Li, Jiaqing Xiong, Jian Chen conducted the triboelectric performance tests and commented on the working mechanisms. Yi Li and Dace Gao tested the tensile properties of the membranes. Pooi See Lee and Xiaoxing Zhang supervised this project. All the authors discussed and commented on the manuscript.

Competing financial interests: The authors declare no competing interests.

Appendix A. Supporting Information

References

[1] K. Parida, J. Xiong, X. Zhou, P.S. Lee, Nano Energy. 59 (2019) 237-257.

[2] K. Dong, X. Peng, Z.L. Wang, Adv. Mater. 32 (2020) 1902549.

[3] J. Wang, S. Li, F. Yi, Y. Zi, J. Lin, X. Wang, Y. Xu, Z.L. Wang, Nat. Commun. 7 (2016) 12744.

[4] M.F. Lin, J. Xiong, J. Wang, K. Parida, P.S. Lee, Nano Energy. 44 (2018) 248-255.

[5] L. Zhou, D. Liu, J. Wang, Z.L. Wang, Friction. 8 (2020) 481-506.

[6] Q. Guan, G. Lin, Y. Gong, J. Wang, W. Tan, D. Bao, Y. Liu, Z. You, X. Sun, Z. Wen, Y. Pan, J. Mater. Chem. A. 7 (2019) 13948-13955.

[7] J. Wang, C. Wu, Y. Dai, Z. Zhao, A. Wang, T. Zhang, Z.L. Wang, Nat. Commun. 8 (2017) 88.

[8] C. Yan, Y. Gao, S. Zhao, S. Zhang, Y. Zhou, W. Deng, Z. Li, G. Jiang, L. Jin, G. Tian, T. Yang, X. Chu, D. Xiong, Z. Wang, Y. Li, W. Yang, J. Chen, Nano Energy. 67 (2020) 104235.

[9] Z. Cong, W. Guo, Z. Guo, Y. Chen, M. Liu, T. Hou, X. Pu, W. Hu, Z. L. Wang, ACS Nano. 14 (2020) 5590-5599.

[10] D. Liu, X. Yin, H. Guo, L. Zhou, X. Li, C. Zhang, J. Wang, Z.L. Wang, Sci. Adv. 5 (2019). eaav6437.

[11] J. Xiong, M.F. Lin, J. Wang, S.L. Gaw, K. Parida, P.S. Lee, Adv. Energy Mater. 7 (2017) 1701243.

[12] X. Chen, J. Xiong, K. Parida, M. Guo, C. Wang, C. Wang, X. Li, J. Shao, P.S. Lee, Nano Energy. 64 (2019) 103904.

[13] K. Dong, X. Peng, J. An, A.C. Wang, J. Luo, B. Sun, J. Wang, Z.L. Wang, Nat. Commun. 11 (2020) 2868.

[14] Y. Chen, X. Pu, M. Liu, S. Kuang, P. Zhang, Q. Hua, Z. Cong, W. Guo, W. Hu, Z.L. Wang, ACS Nano. 13 (2019) 8936-8945.

[15] X. Liang, T. Jiang, G. Liu, Y. Feng, C. Zhang, Z.L. Wang, Energy Environ. Sci. 13 (2020) 277-285.

[16] H. Chen, Y. Song, X. Cheng, H. Zhang, Nano Energy. 56 (2019) 252-268.

[17] F. Huang, H. Yu, S. Xiang, J. Xue, H. Ming, C. Tao, N. Zhang, X. Fan, ACS Appl. Mater. Interfaces. 12 (2020) 3654-3660.

[18] T.G. Yun, J. Bae, A. Rothschild, I.D. Kim, ACS Nano. 13 (2019) 12703-12709.

[19] J. Shi, S. Liu, L. Zhang, B. Yang, L. Shu, Y. Yang, M. Ren, Y. Wang, J. Chen, W. Chen, Y. Chai, X. Tao, Adv. Mater. 32 (2020) 1901958.

[20] J.W. Lee, S. Jung, T.W. Lee, J. Jo, H.Y. Chae, K. Choi, J.J. Kim, J.H. Lee, C. Yang, J.M. Baik, Adv. Energy Mater. 9 (2019) 1901987.

[21] J. Xiong, H. Luo, D. Gao, X. Zhou, P. Cui, G. Thangavel, K. Parida, P.S. Lee, Nano Energy. 61 (2019) 584-593.

[22] H. Guo, J. Wan, H. Wu, H. Wang, L. Miao, Y. Song, H. Chen, M. Han, H. Zhang, ACS Appl. Mater. Interfaces. 12 (2020) 22357-22364.

[23] J. Xiong, G. Thangavel, J. Wang, X. Zhou, P.S. Lee, Sci. Adv. 6 (2020) eabb4246.

[24] N. Zhang, F. Huang, S. Zhao, X. Lv, Y. Zhou, S. Xiang, S. Xu, Y. Li, G. Chen, C. Tao, Y. Nie, J. Chen, X. Fan, Matter. 2 (2020) 1260-1269.

[25] J. Xiong, P. Cui, X. Chen, J. Wang, K. Parida, M.F. Lin, P.S. Lee, Nat. Commun. 9 (2018) 1-9.

[26] K. Meng, S. Zhao, Y. Zhou, Y. Wu, S. Zhang, Q. He, X. Wang, Z. Zhou, W. Fan, X. Tan, J. Yang, J. Chen, Matter. 2 (2020) 896-907.

[27] J. Xiong, P.S. Lee, Sci. Technol. Adv. Mater. 20 (2019) 837-857.

[28] N. Zhang, Y. Li, S. Xiang, W. Guo, H. Zhang, C. Tao, S. Yang, X. Fan, Nano Energy. 72 (2020) 104664.

[29] Z. Lin, J. Yang, X. Li, Y. Wu, W. Wei, J. Liu, J. Chen, J. Yang, Adv. Funct. Mater. 28 (2018) 1704112.
[30] X. Pu, M. Liu, X. Chen, J. Sun, C. Du, Y. Zhang, J. Zhai, W. Hu, Z.L. Wang, Sci. Adv. 3 (2017) e1700015.
[31] L. Zheng, S. Dong, J. Nie, S. Li, Z. Ren, X. Ma, X. Chen, H. Li, Z.L. Wang, ACS Appl. Mater. Interfaces. 11 (2019) 42504-42511.
[32] Y. Zou, P. Tan, B. Shi, H. Ouyang, D. Jiang, Z. Liu, H. Li, M. Yu, C. Wang, X. Qu, L. Zhao, Y. Fan, Z.L. Wang, Z. Li, Nat. Commun. 10 (2019) 1-10.
[33] Y.C. Lai, Y.C. Hsiao, H.M. Wu, Z.L. Wang, Adv. Sci. 6 (2019) 1801883.
[34] Z. Li, M. Zhu, J. Shen, Q. Qiu, J. Yu, B. Ding, Adv. Funct. Mater. 30 (2020) 1908411.
[35] J. Zhao, W. Zhu, X. Wang, L. Liu, J. Yu, B. Ding, ACS Nano. 14 (2020) 1045-1054.
[36] V. Sencadas, C. Garvey, S. Mudie, J.J.K. Kirkensgaard, G. Gouadec, S. Hauser, Nano Energy. 66 (2019) 104106.
[37] J.Y. Cheong, M. Mafi, L. Benker, J. Zhu, M. Mader, C. Liang, H. Hou, S. Agarwal, I.D. Kim, A. Greiner, ACS Appl. Mater. Interfaces. 12 (2020) 18002-18011.
[38] X. Wang, Y. Zhang, X. Zhang, Z. Huo, X. Li, M. Que, Z. Peng, H. Wang, C. Pan, Adv. Mater. 30 (2018) 1706738.
[39] X. Liang, T. Zhao, W. Jiang, X. Yu, Y. Hu, P. Zhu, H. Zheng, R. Sun, C.P. Wong, Nano Energy. 58 (2019) 508-516.
[40] A.R. Mule, B. Dudem, H. Patnam, S.A. Graham, J.S. Yu, ACS Sustain. Chem. Eng. 7 (2019) 16450-16458.
[41] Y. Liu, L. Wang, L. Zhao, K. Yao, Z. Xie, Y. Zi, X. Yu, Adv. Electron. Mater. 6 (2020) 1901174.
[42] J. Yu, X. Hou, J. He, M. Cui, C. Wang, W. Geng, J. Mu, B. Han, X. Chou, Nano Energy. 69 (2020) 104437.
[43] F. Liang, X.J. Zhao, H.Y. Li, Y.J. Fan, J.W. Cao, Z.L. Wang, G. Zhu, Nano Energy. 69 (2020) 104414.
[44] L. Zhu, X. Zhou, Y. Liu, Q. Fu, Highly Sensitive, ACS Appl. Mater. Interfaces. 11 (2019) 12968-12977.
[45] L. Liu, H.Y. Li, Y.J. Fan, Y.H. Chen, S.Y. Kuang, Z. Bin Li, Z.L. Wang, G. Zhu, Small. 15 (2019) 1900755.

[46] Y.J. Fan, X. Li, S.Y. Kuang, L. Zhang, Y.H. Chen, L. Liu, K. Zhang, S.W. Ma, F. Liang, T. Wu, Z.L. Wang, G. Zhu, ACS Nano. 12 (2018) 9326-9332.
[47] Y. Guo, W. Zhou, L. Wang, Y. Dong, J. Yu, X. Li, B. Ding, ACS Appl. Bio Mater. 2 (2019) 5949-5956.
[48] N. Zheng, Y. Song, L. Wang, J. Gao, Y. Wang, X. Dong, Ind. Eng. Chem. Res. 58 (2019), 15470-15478.
[49] Y. Ertas, T. Uyar, Carbohydr. Polym. 177 (2017) 378-387.
[50] M. W. Matsen, F. S. Bates, Macromolecules. 29 (1996) 7641-7644.
[51] M. W. Matsen, F. S. Bates, Macromolecules. 29 (1996) 1091-1098.
[52] L. Wang, P.D. Topham, O.O. Mykhaylyk, H. Yu, A.J. Ryan, J.P.A. Fairclough, W. Bras, Macromol. Rapid Commun. 36 (2015) 1437-1443.
[53] J. P. Lee, J. W. Lee, J. M. Baik, Micromachines. 9 (2018) 532.
[54] X. Yang, Y. Wang, X Qing, Sensors Actuators, A Phys. 299 (2019) 111579.
[55] H. Kang, H. Kim, S. Kim, H.J. Shin, S. Cheon, J.H. Huh, D.Y. Lee, S. Lee, S.W. Kim, J.H. Cho, Adv. Funct. Mater. 26 (2016) 7717-7724.
[56] S. Oberoi, D. Sonawane, P. Kumar, Compos. Sci. Technol. 127 (2016) 185-192.
[57] S.M. Daghash, O.E. Ozbulut, Mater. Des. 111 (2016) 504-512.
[58] R. Menini, M. Farzaneh, Polym. Int. 51 (2008) 77-84.
[59] Y. Si, Z. Dong, L. Jiang, ACS Cent. Sci. 4 (2018) 1102-1112.
[60] J. Xue, T. Wu, Y. Dai, Y. Xia, Chemical Reviews. 119 (2019) 5298-5415.
[61] Y. Li, Z. Zhu, J. Yu, B. Ding, ACS Appl. Mater. Interfaces. 7 (2015) 13538-13546.
[62] J. Wang, G. Cai, S. Li, D. Gao, J. Xiong, P. S. Lee, Adv. Mater. 30 (2018) 1706157.
[63] Y. Yang, J. Han, J. Huang, J. Sun, Z. L. Wang, S. Seo, Q. Sun, Adv. Funct. Mater. 30 (2020) 201909652.
[64] C. Wu, T. W. Kim, J. H. Park, B. Koo, S. Sung, J. Shao, C. Zhang, Z. L. Wang, ACS Nano. 14 (2020) 1390-1398.
[65] Z. L. Wang, Nano Energy. 68 (2020) 104272.

Mr. Yi Li received his bachelor degree from Wuhan University in 2012. Now he a Ph.D. candidate in the School of Electric Engineering and Automation, Wuhan University. He is also a visiting graduate in the School of Materials Science and Engineering, Nanyang Technological University. His research focus on SF_6 alternative gas, triboelectric nanogenerators and self-powered sensors for smart power system.

Dr. Jiaqing Xiong received his Ph.D. from Soochow University in 2015. Now he is a senior research fellow in the School of Materials Science and Engineering, Nanyang Technological University. His research focuses on smart fibers/textiles, flexible and wearable devices, and functional materials for self-powered systems and human-machine interface.

Dr. Jian Lv received his Ph.D in Material Science and Engineering at Xi'an Jiaotong University in June 2019. During 2017-2019, he was a visiting graduate and then a research associate at University of California, San Diego. He is currently a research fellow at the Nanyang Technological University, Singapore. His main research interests involve the printed wearable and stretchable devices with the applications in energy harvesting/storage and health care monitoring.

Dr. Jian Chen received his B.S. degree in Central South University in 2014, and his Ph.D. degree in Condensed Matter Physics from University of Chinese Academy of Sciences in 2019. Now he is a postdoctoral fellow in Nanyang Technological University. His research interests include triboelectric nanogenerators, self-powered systems and soft robot.

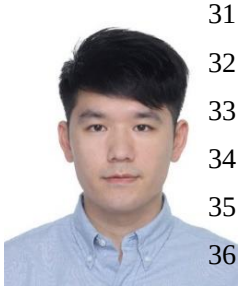

Mr. Dace Gao received his B.Eng. from ZheJiang University in 2016. He is currently a PhD student under the supervision of Prof. Lee Pooi See at Nanyang Technological University. His research interests include additive manufacturing, soft electronics, and soft robotics.

Prof. Xiaoxing Zhang received his Bachelor and Master degrees from Hubei University of Technology, and Doctor degree from Chongqing University. He is currently a professor of School of Electrical and Electronic Engineering, Hubei University of Technology. His research focus in the online monitoring and fault diagnosis of high voltage electrical insulation equipment, SF_6 alternative gases and gas sensors.

Prof. Pooi See Lee received her Ph.D. from National University of Singapore in 2002. She joined the School of Materials Science and Engineering, Nanyang Technological University as an Assistant Professor in 2004. She was promoted to tenured Associate Professor in 2009 and full Professor in 2015. Her research focuses on nanomaterials for energy and electronics applications, flexible and stretchable devices, electrochemical inspired devices, and human-machine interface. She received the National Research Foundation Investigatorship Award and the Nanyang Research Excellence Award in 2016.